Non-linear modulation of short wavelength compressional Alfvén eigenmodes

E. D. Fredrickson,[1] N. N. Gorelenkov,[1] M. Podesta,[1] A. Bortolon,[2] N. A. Crocker,[3] S. P. Gerhardt,[1] R. E. Bell,[1] A. Diallo,[1] B. LeBlanc,[1] F. M. Levinton,[4] and H. Yuh[4]

[1]*Princeton Plasma Physics Laboratory, Princeton, New Jersey 08543, USA*
[2]*University of California, Irvine, California 92697, USA*
[3]*University of California, Los Angeles, California 90095, USA*
[4]*Nova Photonics, Princeton, New Jersey 08543, USA*

Most Alfvénic activity in the frequency range between toroidal Alfvén eigenmodes and roughly one half of the ion cyclotron frequency on National Spherical Torus eXperiment [Ono *et al.*, Nucl. Fusion **40**, 557 (2000)], that is, approximately 0.3 MHz up to ≈1.2 MHz, are modes propagating counter to the neutral beam ions. These have been modeled as Compressional and Global Alfvén Eigenmodes (CAE and GAE) and are excited through a Doppler-shifted cyclotron resonance with the beam ions. There is also a class of co-propagating modes at higher frequency than the counter-propagating CAE and GAE. These modes have been identified as CAE, and are seen mostly in the company of a low frequency, n = 1 kink-like mode. In this paper, we present measurements of the spectrum of these high frequency CAE (hfCAE) and their mode structure. We compare those measurements to a simple model of CAE and present a predator-prey type model of the curious non-linear coupling of the hfCAE and the low frequency kink-like mode. © 2013 AIP Publishing LLC
[http://dx.doi.org/10.1063/1.4801663]

I. INTRODUCTION

The National Spherical Torus eXperiment (NSTX) is a medium size (major radius ≈ 0.85 m, minor radius ≈ 0.65 m), low aspect ratio tokamak capable of toroidal fields up to 5.6 kG and plasma currents up to 1.4 MA.[1] The plasma can be heated with up to 6 MW of deuterium neutral beams, which are injected with energies from ≈60 keV up to 90 keV. At these energies, the beam ion velocities are several times the Alfvén velocity over the typical ranges of plasma density and magnetic field. The super-Alfvénic fast ion population routinely excites a broad spectrum of MHD and Alfvénic mode activity. The instabilities that are the focus of this paper are co-propagating (propagating in the same direction as the beam ion injection) Compressional Alfven eigenmodes (CAEs) seen in beam heated H-mode plasmas at frequencies above the ctr-propagating Global Alfvén eigenmodes (GAE) and CAE, between roughly 1.2 MHz and 2.5 MHz (Fig. 1(a)).

Figure 1 shows spectrograms of a Mirnov coil signal covering three frequency bands, each with its own assortment of modes as identified in the figures. In the highest frequency band, Fig. 1(a) is an example of the multiple co-propagating CAE to be discussed here.[2,3] For convenience, these co-propagating CAE will be referred to as "high frequency CAE" or hfCAE to differentiate from the lower frequency, counter-propagating CAE and GAE. The ion cyclotron frequency on the outboard midplane is 2.17 MHz. The intermediate frequency band (Fig. 1(b)) is populated largely by what are believed to be counter-propagating CAE and GAE. These modes exhibit a broad range of behaviors, including bursting, frequency chirping, avalanching of GAE, and continuous mode activity.[4–9] The drive for these modes is through the

resonance condition $\omega = \omega_{ci} + k_{//}V_{b//}$, where ω, $\omega_{ci} > 0$ and $k_{//}V_{b//} < 0$, and $V_{b//}$ is the beam ion parallel velocity. In the low frequency band are Toroidal Alfvén Eigenmodes (TAE), reversed-shear Alfvén Eigenmodes (rsAE), and a variety of kink and fishbone-like modes (Fig. 1(c)). Similar modes, from TAE up to the co-propagating hfCAE, have also been seen in the beam heated, low aspect ratio MAST[10–13] and the first observations of the broad spectrum of Alfvénic activity were made on START.[13,14] Experimental and theoretical efforts are underway to characterize these various modes, understand the mechanisms for excitation of the modes, how apparently disparate modes interact, and how these modes affect the fast ion population.[15–29]

The hfCAE typically consist of a cluster of up to seven or eight modes, spaced of order 100 kHz apart and with toroidal mode numbers increasing sequentially with increasing frequency. Typically, the toroidal mode numbers are in the range from n ≈ 6 to n ≈ 14. The mode frequency spacing, and other characteristics discussed below, will be shown to be consistent with a simple dispersion relation for CAE. The presence of these modes is highly correlated with a low frequency kink-like mode which often appears at the end of the current ramp-up phase as the q-profile is relaxing. It is postulated that the low frequency kink mode modifies the fast ion distribution, populating the region of fast ion phase space resonant with the hfCAE.[30] However, as will be seen, there is also some evidence for a more direct interaction.

Figures 2 and 3 show some details of the equilibrium plasma in which these modes are seen. In Fig. 2(a), the plasma current reaches the target flattop value of 0.8 MA at about 0.2 s. Neutral beam heating starts early in the current ramp phase to heat the plasma, assist current ramp-up with beam driven current, and to trigger an early H-mode
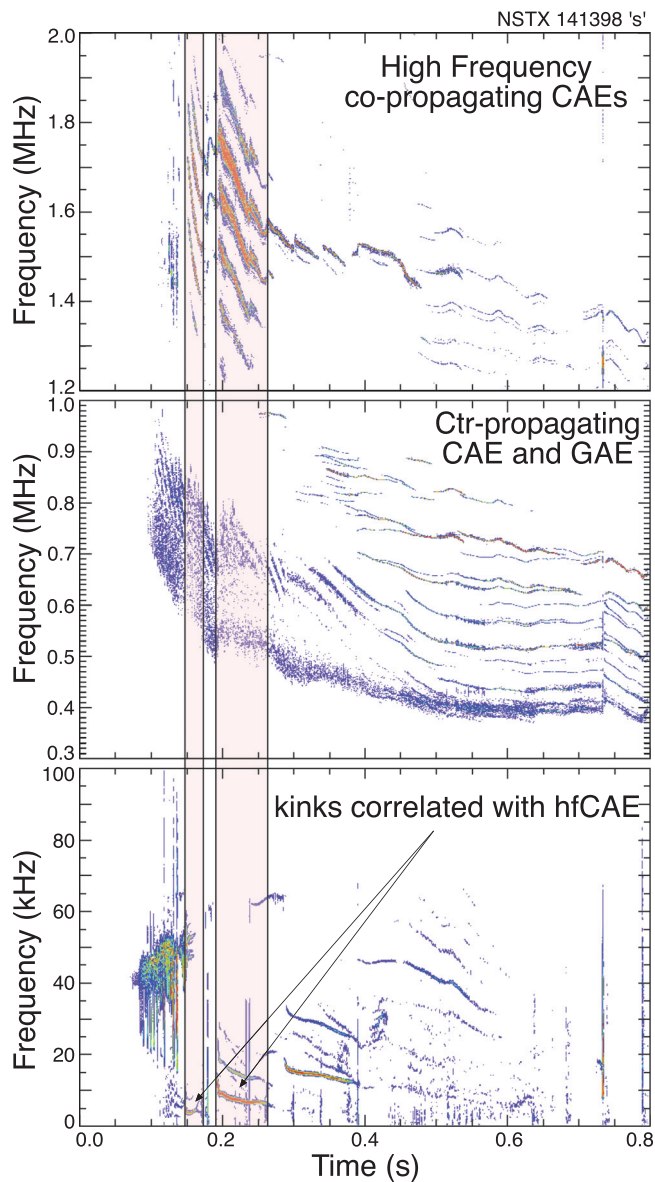
FIG. 1. Spectrograms of magnetic fluctuations; (a) co-propagating, high frequency CAE, (b) ctr-propagating CAE and GAE, (c) rsAE, TAE, and kink-like modes.
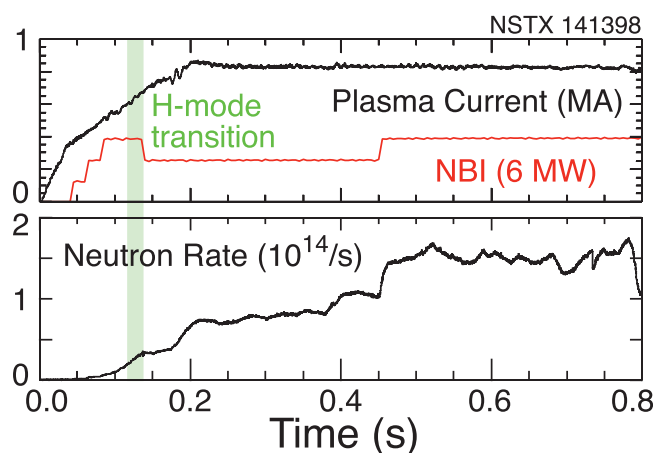

FIG. 2. (a) Plasma current and beam power evolution in time, peak beam power was 6 MW. (b) Neutron rate in time.

transition (at ≈ 0.1 s, green bar). The neutron rate, Fig. 2(b), provides a constraint, through TRANSP modeling, on the beam-ion beta.

The radial profiles of the electron density, rotation frequency, and q-profile at the time of the hfCAE activity are shown in Fig. 3. The very flat density profile, Fig. 3(a), is common in the early period of H-modes on NSTX, and precludes internal measurement of the mode profiles with the reflectometer array. The modes of interest here, the hfCAE, have so far only been seen in H-mode plasmas with flat or even hollow density profiles. The rotation profile, Fig. 3(b), shows relatively slow toroidal rotation. In the region of peak simulated CAE amplitude (blue region) around $R = 1.3$ m, the rotation frequency is about 6 kHz. The kink frequency is similar to the core rotation frequency of ≈ 8–10 kHz. As this is near the end of the current ramping phase, the current profile is still hollow.

The magnetic fluctuations are measured with Mirnov coils. The Mirnov coil array provides good relative phase and amplitude measurements to frequencies greater than 2 MHz. The phase measurements from a toroidal array are used to derive the toroidal mode number n. A limited poloidal array provides some information on the poloidal structure in the outboard-midplane region. The phase and amplitude measurements, including coils measuring toroidal magnetic
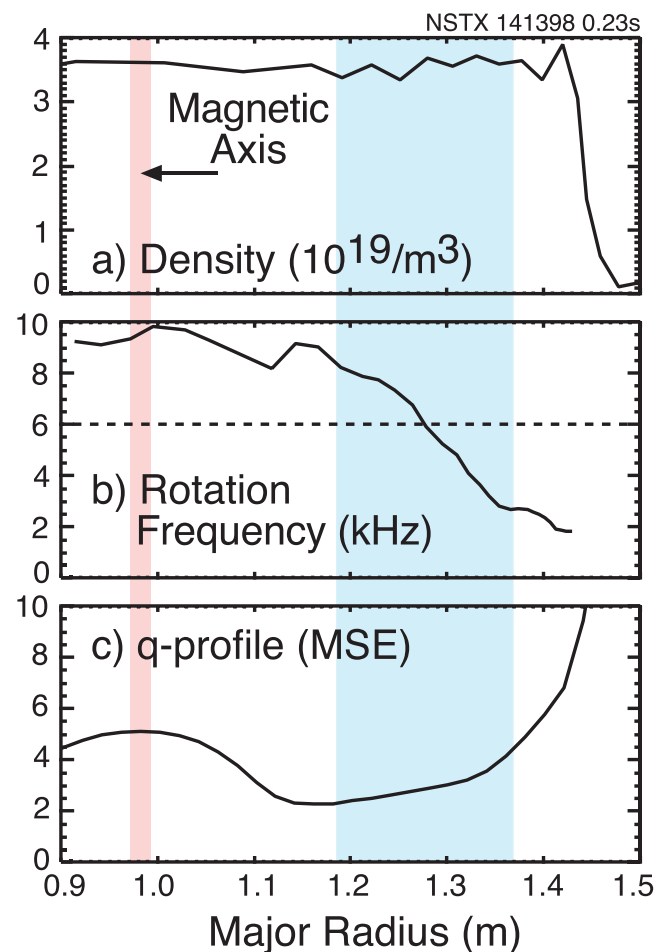

FIG. 3. (a) Flat density profile typical of early phase of NSTX H-modes. (b) Rotation profile reaching ≈ 10 kHz on axis, and (c) typical reversed-shear q-profile as reconstructed from MSE data.
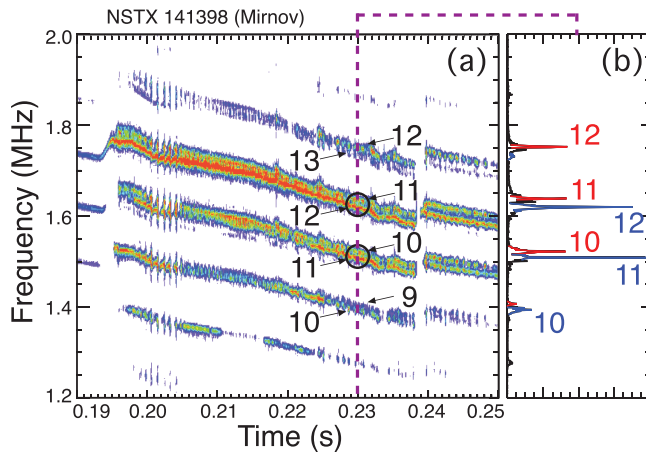
FIG. 4. Detail of spectrogram in Fig. 1, showing detail of high frequency, co-propagating CAE cluster. Toroidal mode numbers are indicated.

fluctuations, are further used to show the shear vs. compressional polarization of the magnetic fluctuations at the plasma edge.

In this paper, we report largely on the experimental characteristics of the class of modes with frequencies typically between ≈ 1.2 MHz and ≈ 2.4 MHz, or up to approximately the deuterium ion cyclotron frequency, seen in beam heated H-mode plasmas. In Sec. II of this paper, experimentally determined characteristics of the hfCAE will be presented, including toroidal mode numbers and some limited information on the poloidal structure. In Sec. III, the mode structure and dispersion relation will be compared to a simple model of CAE. In Sec. IV, an interesting (and unexplained) coupling between the CAE burst frequency and the kink frequency will be demonstrated, and Sec. V will summarize and discuss the observations.

II. CHARACTERISTICS OF THE hfCAE

The spectrogram in Fig. 4 shows the hfCAE in greater detail. Five strong frequency bands, with at least two more weak bands, one at higher frequency, the other at lower frequency, are seen in Fig. 4(a). Each frequency band consists

of at least two modes with significant amplitude (Fig. 4(b)). This example, with the more complicated double peak in each band, was chosen to provide the opportunity for a more extensive comparison with theoretical predictions. Analysis of the two peaks in each frequency band in Fig. 4 find that there is a double sequence of ascending mode numbers (colored blue and red here) as indicated in Fig. 4(b), with the modes in each of the sequences having different, unique characteristics. Subsequently, we will refer to them as the "blue" and "red" sequences, with the blue sequence having larger amplitude on the Mirnov coils.

In the following analysis, we will focus on the two strongest bands in the spectrum shown in Fig. 4(b). The modes include the $n = 11$ and $n = 12$ peaks highlighted in blue at 1.508 MHz and 1.619 MHz, respectively; the corresponding peaks from the "red" band are at 1.522 MHz and 1.638 MHz with, respectively, toroidal mode numbers $n = 10$ and $n = 11$. The modes are propagating in the co-direction, that is, co-parallel to the plasma current and the beam injection. The polarization (shear vs. compressional) analysis and some information on the poloidal structure of the modes are shown in Figs. 5 ("blue" sequence) and 6 ("red" sequence). The poloidal variation of the amplitude of the magnetic fluctuations shown in Fig. 5(b) and the phase step in Fig. 5(a) suggest that the lower frequency (blue) sequence has a standing wave structure with a midplane node, consistent, as will be seen, with models of the CAE. The data shown in Figs. 6(a) and 6(b) for the "red" sequence are more consistent with a combination of a standing wave with an antinode on the midplane combined with a poloidally propagating wave of about half the amplitude, as indicated by the fitted curves in Fig. 6. This interpretation, although consistent with the data, is by no means definitive. The poloidal array spans a fairly narrow range of poloidal angle and consists of only four coils.

The polarization data are shown in Figs. 5(c) and 6(c) as a composite Lissajous diagram for each of the modes. The Lissajous figures are constructed using the poloidal and toroidal magnetic fluctuation amplitudes, together with the relative phase shift between the poloidal and toroidal
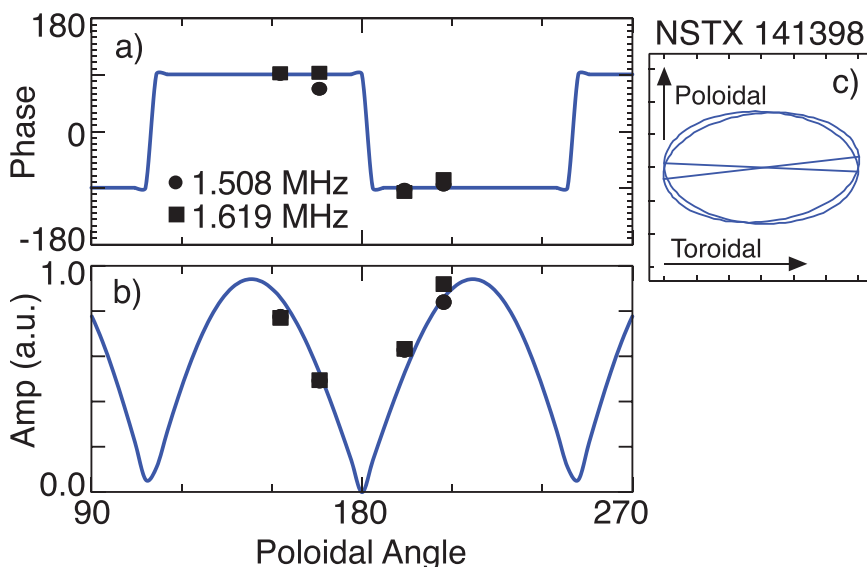

FIG. 5. Poloidal structure and polarization of the 1.51 MHz (solid circles) and 1.62 MHz modes (solid squares); (a) relative phase compared to phase of standing wave for both modes, (b) normalized amplitude compared to amplitude of standing wave, solid lines are fits to the data assuming a standing wave, (c) Lissajous figure showing mixed shear and compressional polarization for both modes.
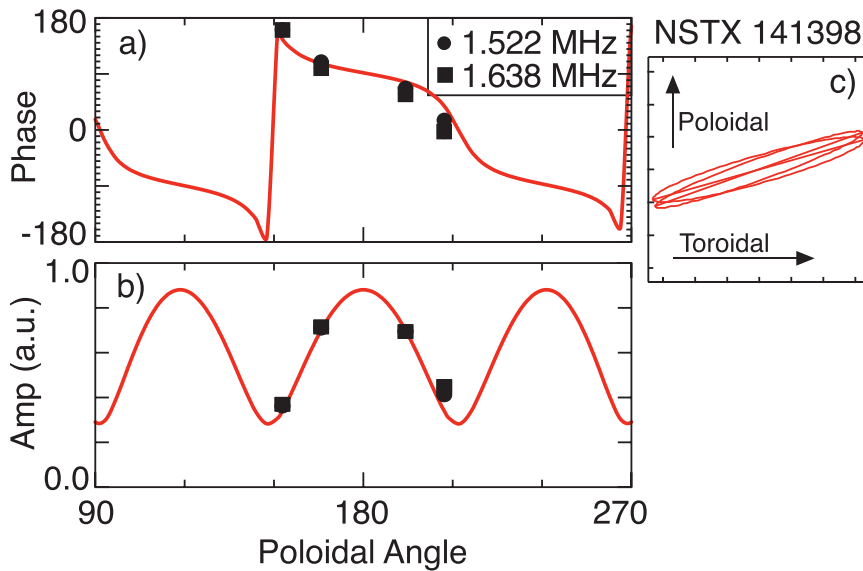
FIG. 6. Poloidal structure and polarization of the 1.52 MHz (solid circles, partially obscured by squares) and 1.64 MHz modes (solid squares); (a) relative phase, (b) normalized amplitude for same two modes, solid lines are fits to the data assuming a mix of standing and propagating waves, (c) Lissajous figures showing compressional polarization for both modes.

components of the magnetic fluctuation. The polarization of the magnetic fluctuations distinguishes between shear or compressional waves, however, the measurement with the Mirnov coils only provides the polarization near the plasma edge; the polarization of modes varies with plasma radius in simulations.[28,29] The blue, lower frequency series (and indeed, the most commonly seen hfCAE), consistently shows an elliptical polarization, although still predominantly compressional. The higher frequency series (red), in this case and others, is consistently more purely compressional, evidenced by the narrower ellipse oriented roughly parallel to the equilibrium magnetic field.

Unlike the counter-propagating CAE and GAE, the hfCAE must satisfy a simpler resonance condition, $\omega \approx k_{//} V_{b//}$ (as $\omega < \omega_{ci}$). The hfCAE typically have larger $k_{//}$ than the lower frequency GAE and CAE, but the resonance condition points to a region of fast ion phase space lightly populated in classical beam deposition and slowing down calculations. In Fig. 7, the resonance condition for the hfCAE are overlaid on the (unperturbed) fast ion distribution as calculated in the TRANSP code.

III. MODEL OF hfCAE BASED ON SIMPLE DISPERSION RELATION

The modes in the frequency range between 1.2 MHz and 2 MHz have been identified as CAE based largely on comparison of the spectrum with the dispersion relation for CAE. In this section, the observed mode spectrum, toroidal mode numbers, and some limited data on poloidal structure will be compared with solutions of a simplified Alfvén wave dispersion relation. The frequency dependence on toroidal mode number is relatively easily compared as the toroidal wavelength is accurately measured. The experimental data on the poloidal mode structure are limited, but sufficient to identify the modes as either up-down symmetric or anti-symmetric, as described earlier. It has not been possible to compare internal measurements of the mode profiles with theoretical predictions, as invariably this band of modes is only present when the density is either nearly flat or even hollow (inside

the pedestal), precluding measurements of mode structure with the reflectometer.

The dispersion relation for Alfvén waves is isotropic at low frequency, $\omega \ll \omega_{ci}$, that is, waves propagating parallel or perpendicular to the magnetic field follow the same dispersion relation, making the finding of eigenmodes (albeit with a very simplified dispersion relation) relatively easy[5,17,22,31] The nominal axisymmetry of tokamaks allows a clean separation of the toroidal variable with the introduction of the toroidal mode number, n. Beginning with the basic Alfvén wave dispersion relation,

$$V_{Alfvén}^2 \nabla^2 E = \frac{\partial^2}{\partial t^2} E, \qquad (1)$$

and separating the toroidal and perpendicular parts in cylindrical geometry (R, z, φ),
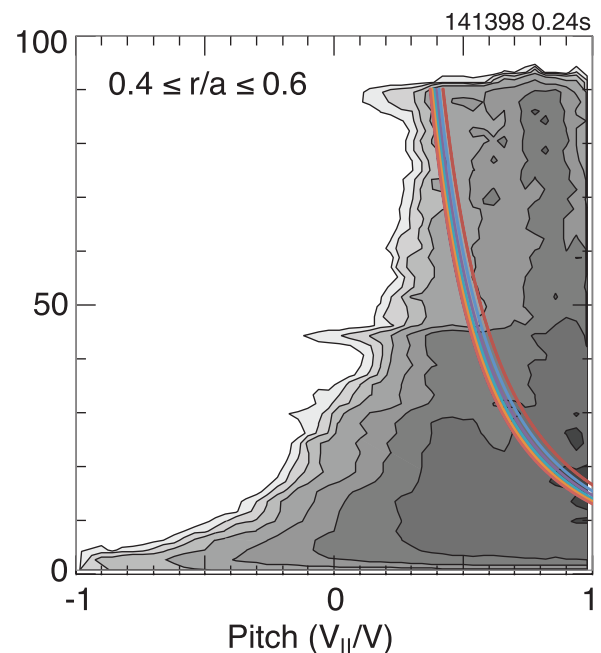

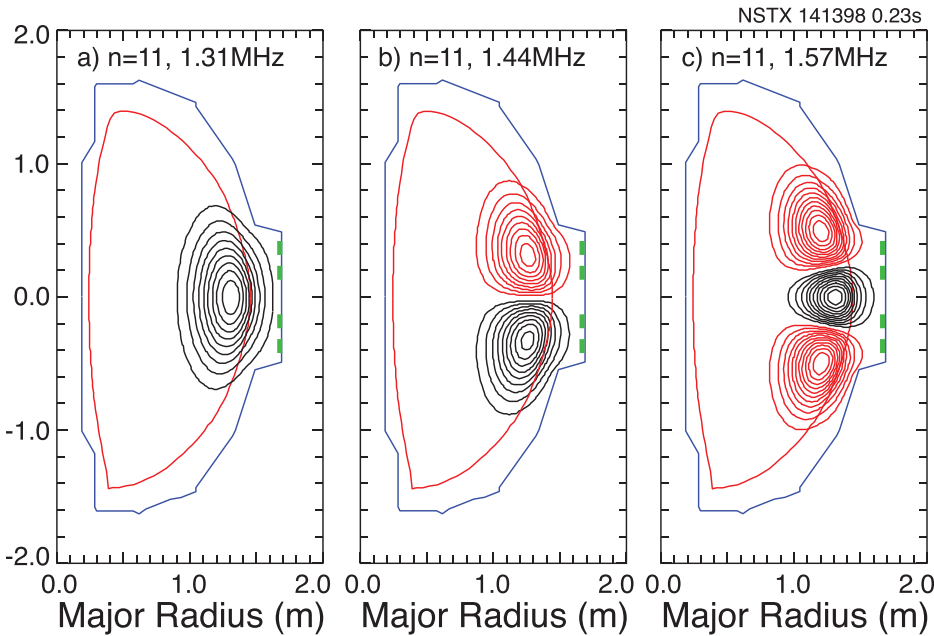FIG. 7. Fast ion distribution calculated by TRANSP at the midradius, near peak in calculated hfCAE mode amplitude.

FIG. 8. Approximate eigenmodes for the first three poloidal eigen-states with n = 11. (a) The lowest order n = 11 poloidal eigen-state, (b) the second order n = 11 poloidal eigen-state, and (c) the third order n = 11 poloidal eigen-state.

$$V_{Alfvén}^2 \left[\nabla_\perp^2 - \frac{n^2}{R^2} \right] E = -\omega^2 E, \qquad (2)$$

yields a 2-D wave equation with a potential well

$$\nabla_\perp^2 E + V(\omega, R, z)E = 0, \qquad (3)$$

$$V(\omega, R, z) = \frac{\omega^2}{V_{Alfvén}^2} - \frac{n^2}{R^2}. \qquad (4)$$

In practice, we are looking for the lowest frequency solutions, thus the well term will be negative where the Alfvén velocity is high and the waves will be evanescent. Thus, this perpendicular part of the wave equation describes standing waves trapped in a 2-D potential well.

The perpendicular part of the dispersion relation is not so easily separated, although approximate solutions have been found.[17,31] Here, we describe solutions by solving the perpendicular, two dimensional equation numerically. The solutions to the 2-D wave equation can easily be found by converting Eq. (3) to a diffusion equation through the addition of a "dummy" term,

$$\nabla_\perp^2 E + V(\omega, R, z)E = \frac{\partial}{\partial \tau} E. \qquad (5)$$

Here, the potential well, $V(\omega, R, z)$, functions as a source term in the diffusion equation.

The numerical calculation starts with an initial guess for the eigenfunction, and the diffusion equation is iterated until the r.h.s. term is effectively zero, thus satisfying the original dispersion relation. At each step, the mode frequency, imbedded in the potential term, is adjusted to minimize the r.h.s., and then the shape of the eigenfunction is adjusted. In practice, the frequency converges quickly, the eigenfunction shape more slowly. At each step, the boundary conditions are enforced (zero amplitude at the "wall") with amplitude rescaled to avoid "zero" solution. This approach works well

for finding the lowest order poloidal eigen-state, which we label by m = 0.5 (m is the number of standing poloidal wavelengths in the eigen-state) shown in Fig. 8(a). Higher order, orthogonal, solutions are found by eliminating the lower order eigen-state components from the solution at each step.

The solutions for a given toroidal mode number alternate between up-down symmetric (even) and up-down anti-symmetric (odd) solutions, corresponding to trapped waves with half-integer wavelengths (m = 0.5, 1.5, 2.5, …) and full integer (m = 1, 2, 3, …) wavelengths in the poloidal direction. Simulations of the n = 11, m = 0.5, 1.0, and 1.5 modes are shown in Fig. 8. For these simulations, the boundary condition, indicated by the blue curves in Fig. 8, for the eigenmode calculation approximates the locations of the passive plates and the vacuum vessel. The Mirnov coil positions and approximate size are indicated in Figs. 8(a)–8(c) by the green rectangles. The experimental poloidal profile of magnetic fluctuations is compared to the simulated magnetic fluctuation profile for the m = 1.0 simulation in Fig. 9. The midplane vertical (poloidal) wavelength appears somewhat shorter than the experimental wavelength.

The frequency spacing of the poloidal eigen-states (m and m + 0.5) is comparable to the frequency spacing of
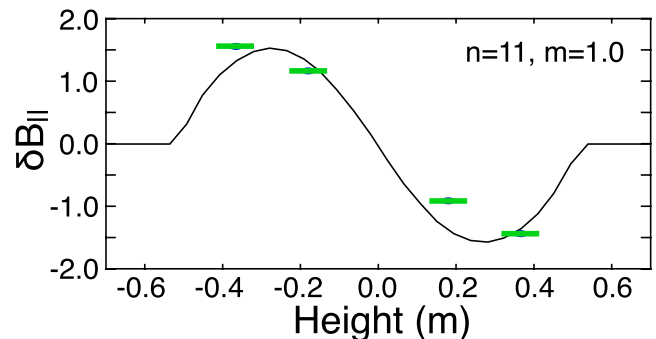

FIG. 9. Comparison of simulated (black line) and experimental (green bars) magnetic fluctuations at the wall for the mode shown in Fig. 8(b).

toroidal harmonics (n and n + 1). Thus, overlapping frequency sequences, alternating between even and odd poloidal structure as seen in the experiment, are consistent with the simulations. The frequencies of the m = 1 modes from n = 9 to n = 13 range from 1.27 MHz for the n = 9 mode up to 1.62 MHz for the n = 13 mode. The experimental frequencies range from 1.28 MHz up to 1.73 MHz, but including a Doppler correction, using a plasma rotation frequency of ≈6 kHz (see Fig. 3), reduces the frequency range from 1.23 MHz to 1.66 MHz, in pretty good agreement with the theoretical calculation (Fig. 10, blue curve). The Doppler-corrected experimental frequencies for the even modes (red sequence) also agree fairly well with the eigenfrequencies for the m = 1.5 poloidal eigen-states (Fig. 10, red curve), although the poloidal measurements suggested at least a partially propagating, rather than standing, wave.

Comparison of the experimental mode spectrum, characteristics of the mode structure (up-down even or odd mode structure) agrees reasonably well with a simple theoretical calculation of mode frequencies and structure. The theoretical calculations of the n = 9 through n = 13 modes for the odd poloidal modes find good agreement with the experimental mode frequencies. The double sequence of modes with even and odd modes is in qualitative agreement with the theoretical modeling.

IV. BURSTING OF hfCAE

The hfCAE are not "constant" amplitude waves, but appear as a sequence of bursts with a burst frequency in the range of a few kHz. This can be seen in Fig. 11, particularly in the time interval from ≈0.2 s to 0.205 s where particularly large, long period bursts are seen. A spectrogram of the absolute value of the magnetic fluctuations in the CAE frequency range shows the burst frequency more clearly (Fig. 11(a)). Fig. 11(b) shows the rms magnetic fluctuation level calculated over the frequency range from 1.2 MHz to 2.0 MHz for
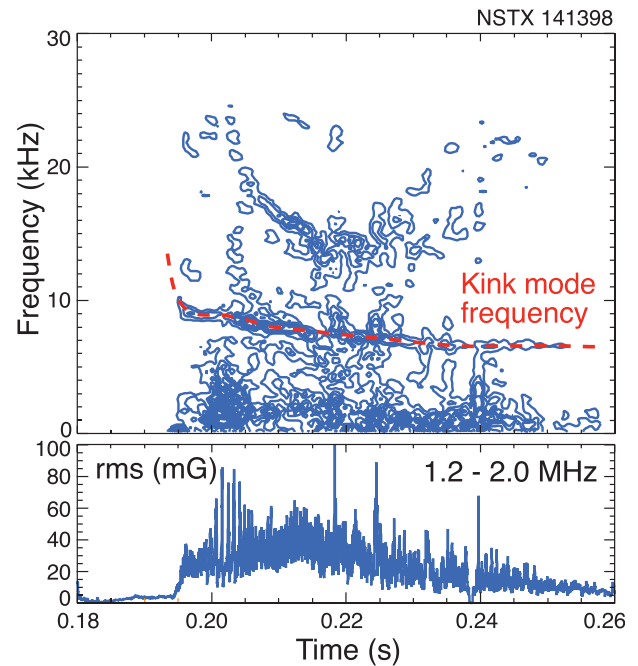

FIG. 11. (a) Spectrogram of rms amplitude of hfCAE in frequency range 1.2 MHz to 2 MHz, (b) rms fluctuation amplitude in frequency range 1.2 MHz to 2 MHz used for spectrogram in (a).

the data shown in Fig. 4. The dashed red curve shows the frequency evolution of the n = 1 kink-like mode. The dominant (natural) burst frequency is at frequencies less than 5 kHz, however, there is significant modulation of the hfCAE burst frequency at the kink mode frequency.

Some features of the bursting and modulation of the burst frequency by the n = 1 kink can be seen more clearly in a second example shown in Fig. 12. This is a more typical case where each frequency band is a single mode, rather than the double sequence of modes as discussed in Sec. II. The hfCAE onset in Fig. 12 follows shortly the appearance of an n = 1 kink-like mode, just as for the example in Fig. 11. In Fig. 12(a) is the spectrogram showing the n = 1 kink and its second harmonic. Fig. 12(b) shows a spectrogram covering the frequency range of the hfCAE where the contour lines are color-coded to indicate the dominant toroidal mode numbers. The color code is indicated in the figure, with black indicating toroidal mode number, n = 8, and red, green, blue, cyan, and magenta n = 9 through 13, respectively.

Fig. 12(c) shows a spectrogram of the hfCAE amplitude. Initially, the natural burst frequency is about 3.5 kHz and the kink frequency is greater than 10 kHz. As the kink frequency drops below ≈6 kHz after 0.235 s, the burst frequency is locked to the kink frequency (dashed black line). The final panel, Fig. 12(d), shows the evolution of the phase between the n = 1 kink and the burst modulation at that frequency, demonstrating that the frequencies are not just close, but are strongly correlated. Before ≈0.235 s, the hfCAE bursts are uncorrelated with the kink, but by 0.24 s they are strongly correlated.

A superficially similar correlation between Toroidal Alfvén eigenmode bursts and a fishbone-like kink has been reported.[32,33] In that case, the TAE bursts were "entrained" in the kink mode; that is multiple TAE formed a wave packet
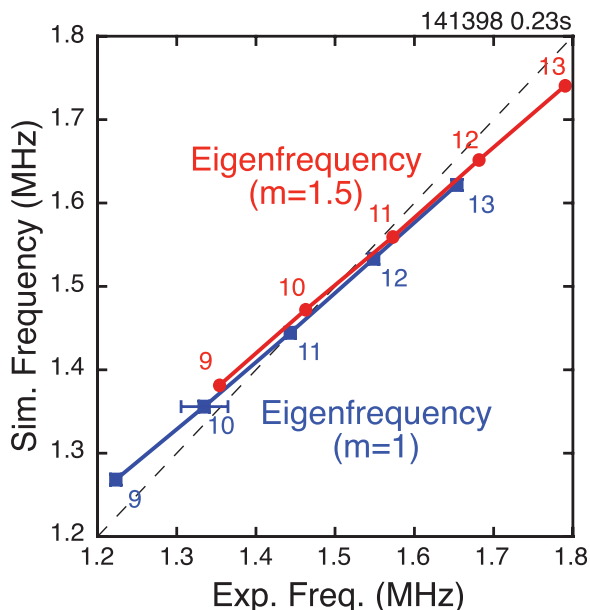

FIG. 10. Comparison of simulated and Doppler-corrected experimental frequencies for m = 1 modes (blue) and m = 1.5 (red).
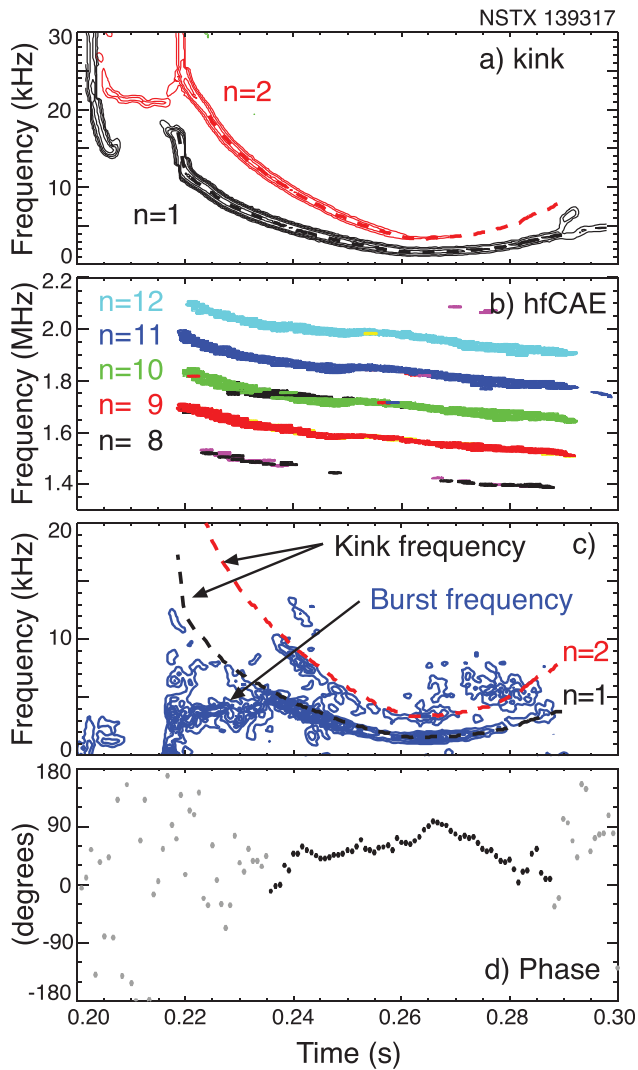
FIG. 12. (a) Spectrogram showing first and second harmonic of n = 1 kink mode, (b) spectrogram showing hfCAE burst correlated with kink, (c) spectrogram of envelope of hfCAE fluctuation amplitude, overlaid with kink mode frequencies, (d) relative phase between n = 1 kind and hfCAE envelope.

FIG. 13. Digitally filtered (1.4–2.0 MHz) signals from each of the three coils separated toroidally by 120°. Each color corresponds to the signal from a different toroidal position, indicated at the top of the figure. Black curves are the kink, filter from 2 to 30 kHz.

that propagated with the kink frequency, appearing as bursts to local measurements (a form of three-wave coupling). The hfCAE bursts, in contrast, are global, not toroidally localized; that is, the bursts occur simultaneously on all coils in the toroidal and poloidal arrays, thus are not a form of three wave coupling. For example, in Fig. 13, the signals from each of three coils separated toroidally by 120° are digitally filtered over the range 1.4 MHz to 2 MHz. The signals are overlaid with the kink oscillation obtained by again digital filtering from 2 kHz to 30 kHz. It is seen that while there are small differences in the shape of the bursts, the bursting is global. In that respect, they are unlike the TAE bursts which were trapped in the n = 1 kink wave and thus toroidally localized, meaning the wave packets (bursts) propagate in the toroidal direction.[32,33] One interpretation of this observation is that the stability of the bursts is being modulated at the n = 1 kink frequency, as explained below.

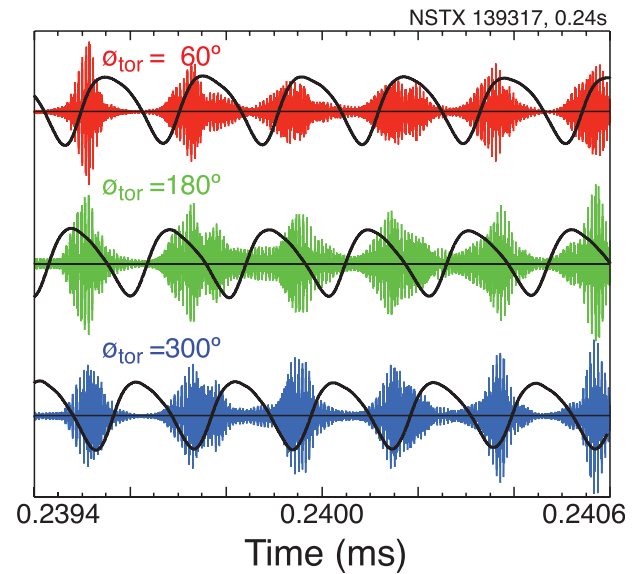The spectrogram of the burst frequency (Fig. 12(c)) was calculated from the rms fluctuation amplitude evolution

averaged over all of the hfCAE modes between 1.4 MHz and 2.0 MHz. Similar spectrograms may be constructed by filtering to extract the evolution of each mode separately. Early it is seen that the bursting of each of the modes, n = 9 through n = 12, are strongly correlated, with bursts separated by quiescent periods (Fig. 14). Here, it appears that the n = 11 mode is triggered first, with the modes at higher and lower frequency triggered later. The simplest explanation is that the n = 11 mode is the least stable, and thus is triggered first by the rising fast ion beta.

Later in time the bursting is not so distinct, with the mode amplitude modulated, but persisting between bursts. There is also weaker correlation of the bursts between modes, with the n = 11 hfCAE most strongly modulated at the kink frequency (Fig. 15).

V. PREDATOR-PREY MODEL OF BURSTING

The repetitive bursting of modes can be simulated with a simple predator-prey model,[34,35] as illustrated in Fig. 16. In this model, the fast ion beta assumes the role of the "prey," increasing linearly with source rate in the absence of mode induced losses. The mode amplitude plays the role of "predator," causing losses of fast ions. The linear drive for the mode is assumed proportional to the fast ion pressure (or more accurately, the number of fast ions resonant with the mode). There is a threshold in fast ion beta, β_c, set by the natural damping rate for the mode, $\partial A/\partial t \sim A\,[\gamma_d(B-1)]$, where A represents the mode amplitude, γ_d is the linear damping rate and $B = \beta_f/\beta_c$ or γ_{drive}/γ_d. The fast ion beta is assumed to evolve as $\partial B/\partial t \sim S - A^2 B$, with S being the source rate of fast ions, and again, β_f represents the number of fast ions resonantly driving the mode. This predicts a linear rise in β_f/β_c, which is approximately correct given the assumption that the equilibrium state (in absence of mode-induced transport) has $\beta_f/\beta_c \gg 1$. Eventually, as the fast ion
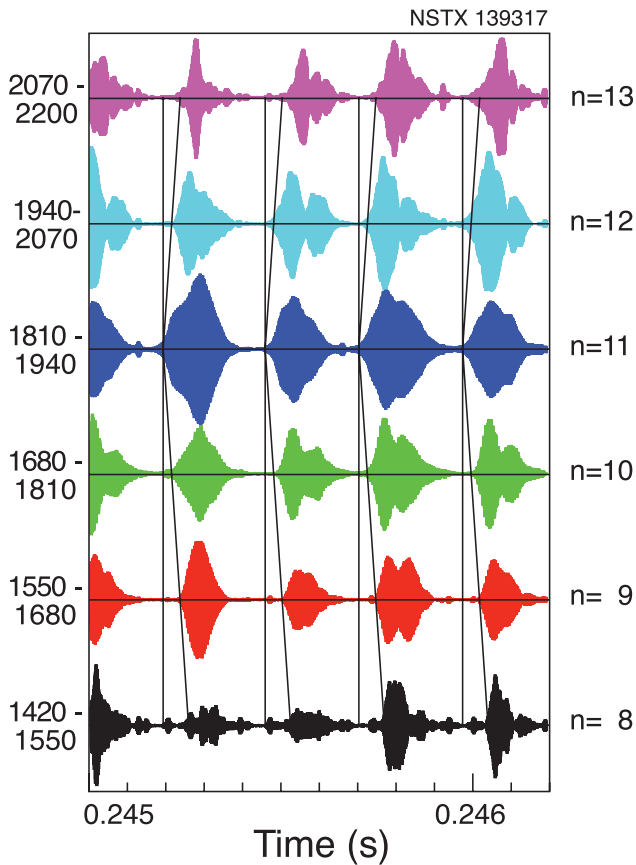
FIG. 14. Filtered Mirnov signal (frequency range on left) showing each hfCAE mode (mode numbers on right. Burst pattern for each mode is different, but all are correlated.

FIG. 16. Predator-prey model simulating coupling of kink to hfCAE.

and the mode amplitude decays. The fast ion beta begins to recover and the cycle repeats. In the simulations described here, the "loss rate" is assumed proportional to the square of the mode amplitude, as for a diffusive loss.[34] Here, loss refers generally to the movement out of resonance with the mode, in phase space, of fast ions. This model will predict a "natural" burst frequency for the modes. We use a modified predator-prey model where either the damping rate or the drive (β_f) is modulated at the kink rotation frequency. As is shown below, a modulation of either drive or damping by as little as 2% can cause locking of the burst frequency to the modulation (kink) frequency when the modulation frequency is close to the natural burst frequency.

The difference equations used in the modified predator-prey code, using the parameters A, B, S, and γ_d as introduced above, are

$$A_{n+1} = \max[10^{-3}, A_n + \gamma_d A_n (B_n - T(t_n))\delta t], \qquad (6)$$

$$B_{n+1} = \max[0, B_n + (S - B_n A_n^2)\delta t]. \qquad (7)$$

Here, A_n represents the normalized mode amplitude and B_n represents the normalized fast ion beta. The fast ion beta is prohibited from being negative, and there is a (small) minimum mode amplitude. Here, the threshold parameter, $T(t_n) = 1 + \delta \sin(\omega_{kink} t)$, allows modulation of the critical beta at the kink frequency. Alternatively, the modulation can be applied to the fast ion beta, B_n. The modulation of the damping rate is postulated to be through a coupling of the kink with a symmetry-breaking error field, however, the mechanism by which this affects the damping or growth rate of the CAE is unclear.

A spectrogram of the burst frequency is shown in Fig. 17 for a predator-prey simulation with parameters chosen to give a "natural" burst frequency of ≈ 5 kHz, similar to the experimental burst frequency. A modulation of 2% is imposed on the damping rate term, with the frequency swept from 10 kHz to 1 kHz over the course of the simulation (black dashed line). Some characteristics of the experimental data (Fig. 12(c)) are then reproduced here. First, when the modulation frequency approaches the "natural" burst frequency, the burst frequency increases to match and track the modulation frequency. Prior to the frequency-capture time, the burst

pressure increases, the drive for the mode (red curve) exceeds the damping rate (blue curve) and the mode (black curve) begins to grow exponentially. As the mode grows, it redistributes fast ions, which eventually removes the drive,
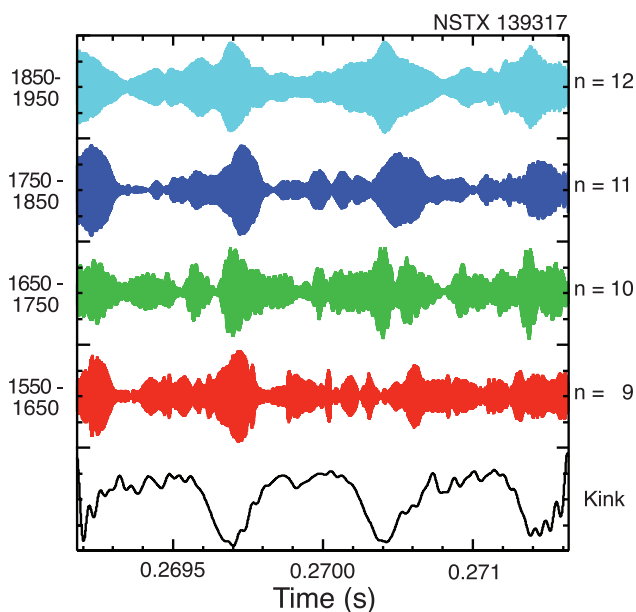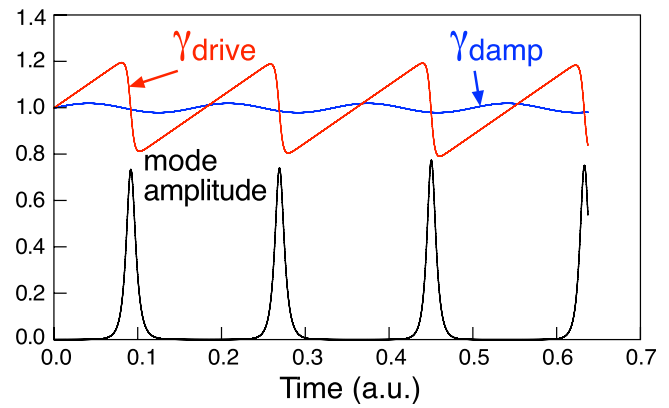

FIG. 15. Filtered Mirnov signal (frequency range on left) showing each hfCAE mode (mode numbers on right. Burst pattern for each mode different, but all are correlated.
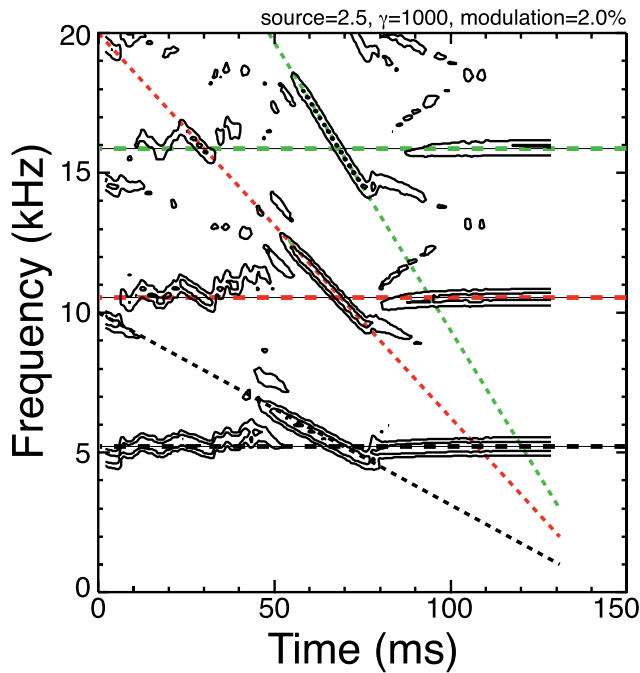
FIG. 17. Spectrogram showing frequency capture from coupling of predator-prey modulations to modulation frequency of critical threshold.

frequency is close to the natural frequency, but is perturbed by higher order resonances with the modulation frequency. This may occur to some extent in the experiment, or the experimental natural burst frequency may not be particularly stable. Unlike the experiment, the frequency-capture fails shortly after the modulation frequency drops below $\approx 80\%$ of the natural burst frequency, and the burst frequency reverts to normal.

This exercise should be viewed as providing a demonstration that modulation of either the drive or damping rate by only a few percent might be sufficient to explain the frequency-capture observed in Figs. 11 and 12.

VI. DISCUSSION

Co-propagating CAE are often seen near the start of the plasma current "flat top" phase. The modes are at higher frequency than the more common counter-propagating global and compressional Alfvén eigenmodes. These hfCAE have frequencies approaching the ion cyclotron frequency. They have only been seen in H-mode plasmas and are very strongly correlated with the presence of a low frequency kink-like mode. Measurements of the magnetic field fluctuation polarization find them dominantly compressional at the plasma boundary, but their identification as CAE rests primarily on comparison of the observed spectrum with the simple CAE dispersion relation. The absolute frequency, the frequency dependence on toroidal mode number and frequency dependence on poloidal mode number, are in good agreement with predictions.

The hfCAE, like most energetic particle driven modes on NSTX, show periodic bursting. When the frequency of the hfCAE bursts is close to the kink frequency, the bursts can become phase-locked to the kink mode. The mechanism

for this coupling is not clear, however, simulations with a predator-prey model find that a modulation of the hfCAE damping rate by a few percent is sufficient to demonstrate the phase-locking seen in the experiment.

ACKNOWLEDGMENTS

[1]M. Ono, S. M. Kaye, Y.-K. M. Peng, G. Barnes, W. Blanchard, M. D. Carter, J. Chrzanowski, L. Dudek, R. Ewig, D. Gates, R. E. Hatcher, T. Jarboe, S. C. Jardin, D. Johnson, R. Kaita, M. Kalish, C. E. Kessel, H. W. Kugel, R. Maingi, R. Majeski, J. Manickam, B. McCormack, J. Menard, D. Mueller, B. A. Nelson, B. E. Nelson, C. Neumeyer, G. Oliaro, F. Paoletti, R. Parsells, E. Perry, N. Pomphrey, S. Ramakrishnan, R. Raman, G. Rewoldt, J. Robinson, A. L. Roquemore, P. Ryan, S. Sabbagh, D. Swain, E. J. Synakowski, M. Viola, M. Williams, J. R. Wilson, and NSTX Team, Nucl. Fusion **40**, 557 (2000).

[2]E. D. Fredrickson, N. A. Crocker, D. Darrow, N. N. Gorelenkov, S. Kubota, M. Podesta, A. Bortolon, S. Gerhardt, R. E. Bell, A. Diallo, B. LeBlanc, F. M. Levinton, and H. Yuh, "Internal amplitude measurements of CAE and GAE," in *38th EPS Conference on Controlled Fusion and Plasma Physics* (ECA, Strasbourg, France, 2011), Vol. 35G, p. 2.119, http://ocs.ciemat.es/EPS2011PAP/pdf/P2.119.pdf.

[3]L. C. Appel, T. Fülöp, M. J. Hole, H. M. Smith, S. D. Pinches, R. G. L. Vann and The MAST Team, "Compressional Alfvén eigenmodes on MAST," Plasma Phys. Control. Fusion **50**, 115011 (2008).

[4]E. D. Fredrickson, N. Gorelenkov, C. Z. Cheng, R. Bell, D. Darrow, D. Johnson, S. Kaye, B. LeBlanc, J. Menard, S. Kubota, and W. Peebles, Phys. Rev. Lett. **87**, 145001 (2001).

[5]E. D. Fredrickson, N. N. Gorelekov, and J. Menard, "Phenomenology of compressional Alfvén eigenmodes," Phys. Plasmas **11**, 3653 (2004).

[6]N. A. Crocker, W. A. Peebles, S. Kubota, J. Zhang, R. E. Bell, E. D. Fredrickson, N. N. Gorelenkov, B. P. LeBlanc, J. E. Menard, M. Podestà, S. A. Sabbagh, K. Tritz, and H. Yuh, "High spatial sampling global mode structure measurements via multichannel reflectometry in NSTX," Plasma Phys. Controlled Fusion **53**, 105001 (2011).

[7]E. D. Fredrickson, N. N. Gorelenkov, E. Belova, N. A. Crocker, S. Kubota, G. J. Kramer, B. LeBlanc, R. E. Bell, M. Podesta, H. Yuh, and F. Levinton, "Observation of global Alfvén eigenmode avalanche events on the National Spherical Torus Experiment," Nucl. Fusion **52**, 043001 (2012).

[8]E. D. Fredrickson, N. N. Gorelenkov, C. Z. Cheng, R. Bell, D. Darrow, D. Gates, D. Johnson, S. Kaye, B. LeBlanc, D. McCune, J. Menard, S. Kubota, and W. Peebles, "Study of the effect of compressional Alfvén modes on thermal transport in the National Spherical Torus Experiment," Phys. Plasmas **9**, 2069 (2002).

[9]E. D. Fredrickson, R. E. Bell, D. S. Darrow, G. Y. Fu, N. N. Gorelenkov, B. P. LeBlanc, S. S. Medley, J. E. Menard, H. Park, A. L. Roquemore, W. W. Heidbrink, S. A. Sabbagh, D. Stutman, K. Tritz, N. A. Crocker, S. Kubota, W. Peebles, K. C. Lee, and F. M. Levinton, "Collective fast ion instability-induced losses in National Spherical Tokamak Experiment," Phys. Plasmas **13**, 056109 (2006).

[10]L. C. Appel, R. J. Akers, R. Martin, and T. Pinfold, "Observation of CAEs on MAST," in *31st EPS Conference on Plasma Physics, London, UK* (Monotypia Franchi, Ciita' di Catelo, Perugia, 2004), Vol. 28G, p. 4.198.

[11]B. Lloyd *et al.* and MAST and NBI teams, "Overview of physics results from MAST," Nucl. Fusion **47**, S658 (2007).

[12]M. P. Gryaznevich *et al.*, "Recent experiments on Alfvén eigenmodes," Nucl. Fusion **48**, 084003 (2008).

[13]M. P. Gryaznevich and S. E. Sharapov, "Perturbative and non-perturbative modes in START and MAST," Nucl. Fusion **46**, S942 (2006).

[14]K. G. McClements, M. P. Gryaznevich, S. E. Sharapov, R. J. Akers, L. C. Appel, G. F. Counsell, C. M. Roach, and R. Majeski, "Physics of energetic particle-driven instabilities in the START spherical tokamak," Plasma Phys. Controlled Fusion **41**, 661 (1999).

[15]N. N. Gorelenkov and C. Z. Cheng, "Alfven cyclotron instability and ion cyclotron emission," Nucl. Fusion **35**, 1743 (1995).

[16]N. N. Gorelenkov and C. Z. Cheng, "Excitation of Alfvén cyclotron instability by charged fusion products in tokamaks," Phys. Plasmas **2**, 1961 (1995).

[17]N. N. Gorelenkov, C. Z. Cheng, and E. Fredrickson, "Compressional Alfven eigenmode dispersion in low aspect ratio plasmas," Phys. Plasmas **9**, 3483 (2002).

[18]N. N. Gorelenkov, C. Z. Cheng, E. Fredrickson, E. Belova, D. Gates, S. Kaye, G. J. Kramer, R. Nazikian, and R. B. White, "Compressional Alfven eigenmode instability in NSTX," Nucl. Fusion **42**, 977 (2002).

[19]N. N. Gorelenkov, E. Fredrickson, E. Belova, C. Z. Cheng, D. Gates, S. Kaye, and R. B. White, in *19th IAEA Fusion Energy Conference, Lyon, France, 14–19 October 2002* (IAEA, Vienna), paper IAEA-CN-94/TH/7-1 Ra.

[20]N. N. Gorelenkov, E. Fredrickson, E. Belova, C. Z. Cheng, D. Gates, S. Kaye, and R. White, "Theory and observations of high frequency Alfvén eigenmodes in low aspect ratio plasmas," Nucl. Fusion **43**, 228 (2003).

[21]E. Belova, N. N. Gorelenkov, C. Z. Cheng, and E. D. Fredrickson, "Numerical study of instabilities driven by energetic neutral beam ions in NSTX," in *Proceedings of the 30th European Physical Society Conference on Controlled Fusion and Plasma Physics, St. Petersburg, Russia, July 2003* (ECA, 2003), Vol. 27A, P. 3.102.

[22]H. Smith, T. Fülöp, and D. Anderson, "Localization of compressional Alfvén eigenmodes in spherical tori," Phys. Plasmas **10**, 1437 (2003).

[23]V. S. Belikov, Ya. I. Kolesnichenko, and R. B. White, "Destabilization of fast magnetoacoustic waves by circulating energetic ions in toroidal plasmas," Phys. Plasmas **10**, 4771 (2003).

[24]E. Hameiri, A. Ishizawa, and A. Ishida, "Waves in the Hall-magnetohydrodynamics model," Phys. Plasmas **12**, 072109 (2005).

[25]N. N. Gorelenkov, E. D. Fredrickson, W. W. Heidbrink, N. A. Crocker, S. Kubota, and W. A. Peebles, "Discrete compressional Alfvén eigenmode spectrum in tokamaks," Nucl. Fusion **46**, S933 (2006).

[26]Ya. Kolesnichenko, R. B. White, and Yu. V. Yakovenko, "High-frequency shear Alfvén instability driven by circulating energetic ions in NSTX," Phys. Plasmas **13**, 122503 (2006).

[27]H. L. Berk, C. J. Boswell, D. Borba, B. N. Breizman, A. C. A. Figueiredo, E. D. Fredrickson, N. N. Gorelenkov, R. W. Harvey, W. W. Heidbrink, T. Johnson, S. S. Medley, M. F. F. Nave, S. D. Pinches, E. Ruskov, S. E. Sharapov, and JET EFDA contributors, "Interpretation of mode frequency sweeping in JET and NSTX," in *Proceedings of the 21st IAEA Fusion Energy Conference, 16–21 October 2006, Chengdu, China* (IAEA, Vienna, 2007), paper IAEA-TH/3-1.

[28]E. V. Belova, N. N. Gorelenkov, and E. D. Fredrickson, "Numerical modeling of NBI-driven GAE modes,"in *APS April Meeting* (Bulletin of the American Physical Society, 2009), abstract #S1.070.

[29]E. V. Belova, N. N. Gorelenkov, E. D. Fredrickson, H. L. Berk, G. J. Kramer, and S. S. Medley, "Numerical simulations of NBI-driven GAE modes in L–mode and H–mode discharges in NSTX." To be published in *Proc. 24th Int. Conf. on Fusion Energy 2012* (San Diego, CA, 8–13 October 2012) (Vienna: IAEA) Paper TH/P6–16, http://fec2012.iaea.org/contributionDisplay.py?contribId=302&sessionId=9&confId=10.

[30]A. Bortolon, "Interplay between coexisting MHD instabilities mediated by energetic ions in NSTX H-mode plasmas," in *54th Annual Meeting of the APS Division of Plasma Physics, October 29–November 2, 2012, Providence, RI* (Bulletin of the American Physical Society, 2012), Vol. 57, No. 12, Abstract JI2.00002, p. 150, http://meeting.aps.org/Meeting/DPP12/Event/175544.

[31]W. W. Heidbrink, E. D. Fredrickson, N. N. Gorelenkov, T. L. Rhodes, and M. A. Van Zeeland, "Observation of compressional Alfvén eigenmodes (CAE) in a conventional tokamak," Nucl. Fusion **46**, 324 (2006).

[32]N. A. Crocker, W. A. Peebles, S. Kubota, E. D. Fredrickson, S. M. Kaye, B. P. LeBlanc, and J. E. Menard, "Three-wave interactions between fast-ion modes in the national spherical torus experiment," Phys. Rev. Lett. **97**, 045002 (2006).

[33]M. Podesta', R. E. Bell, N. A. Crocker, E. D. Fredrickson, N. N. Gorelenkov, W. W. Heidbrink, S. Kubota, B. P. LeBlanc, and H. Yuh, "Non-linear dynamics of toroidicity-induced Alfvén eigenmodes on the National Spherical Torus Experiment," Nucl. Fusion **51**, 063035 (2011).

[34]W. W. Heidbrink, H. H. Duong, J. Manson, E. Wilfrid, and C. Oberman, "The nonlinear saturation of beam-driven instabilities: Theory and experiment," Phys. Fluids B **5**, 2176 (1993).

[35]W. W. Heidbrink, E. Ruskov, E. D. Fredrickson, N. Gorelenkov, S. S. Medley, H. L. Berk, and R. W. Harvey, "Weak effect of ion cyclotron acceleration on rapidly chirping beam-driven instabilities in the national spherical torus experiment," Plasma Phys. Controlled Fusion **48**, 1347 (2006).